# Development of Order-limited Samples on the Sphere

A Masters Thesis
Presented By

Salman Nadeem
20060004

In Partial Fulfillment of the requirements of the degree of
Masters in Electrical Engineering

Supervisor: Dr. Zubair Khalid

Fall 2022


Department of Electrical Engineering
Syed Babar Ali School of Science and Engineering
Lahore University of Management Sciences

This masters thesis has been examined by a Committee of the Department of Electrical Engineering as follows:

Dr. Adeem Aslam .....
Evaluator, Thesis Committee
Professor of Electrical Engineering

Dr. Muhammad Tahir .....
Thesis Co-supervisor
Professor of Electrical Engineering

Dr. Zubair Khalid .....
Thesis Supervisor
Professor of Electrical Engineering

# Acknowledgements

This thesis owes its success to the generous support of many individuals and groups.

- First and foremost, I would like to thank my thesis advisor Dr. Zubair Khalid. He consistently made sure I was going in the right direction while allowing me to take ownership of this work.
- I am profoundly indebted to my research colleague and mentor Muhammad Salaar Arif for his guidance and close supervision. Learning from him was an honour and a privilege.
- I would like to extend my sincere gratitude to my thesis co-advisor Dr. Muhammad Tahir. He was always there when I needed his support – academic or otherwise.
- Finally, I am deeply thankful to my friends and family for their unwavering support and encouragement throughout my studies and while I was researching and writing this thesis. This accomplishment would not have been possible without them.

# Abstract

We formulate and generalize sampling methods on the sphere – based on the Gauss-Legendre (GL) quadrature and Optimal Dimensionality (OD) schemes – that permit high precision calculation of the spherical harmonic transform (SHT) and the inverse spherical harmonic transform (ISHT) for signals band-limited to $L$ and order-limited to $M$ using $L(2M+1)$ and $M^2+(L-M)(2M+1)$ number of samples respectively. Signals that are nearly rotationally symmetric appear in many applications such as geophysics and antenna theory due to natural azimuthal symmetry of the underlying process. For example, temperature variations in the climate data exhibit symmetry for a fixed co-latitude. Such signals when expanded in the spherical harmonic domain do not have strong dependence on spherical coefficients of higher orders. In this work, we propose order-limited species of the aforementioned sampling methods and develop associated SHTs to save the required number of samples and the computation cost while maintaining reasonable signal reconstruction accuracy. We also assess the numerical accuracy and computational complexity of the proposed transforms, and explore their applicability in antenna theory.

# List of Acronyms

| | |
|---|---|
| 1D | 1 dimensional |
| 2D | 2 dimensional |
| 3D | 3 dimensional |
| AS | azimuthally symmetric |
| CMB | cosmic microwave background |
| DH | Driscoll and Healy |
| FFT | fast Fourier transform |
| GL | Gauss-Legendre |
| HEALPix | hierarchical equal area iso-Latitude pixelization |
| ISHT | inverse spherical harmonic transform |
| MW | McEwen and Wiaux |
| NAS | nearly azimuthally symmetric |
| NSHT | novel spherical harmonic transform |
| OD | optimal dimensionality |
| SHB | spherical harmonic basis |
| SHT | spherical harmonic transform |

# Notations

| | |
|---|---|
| $x$ | scalar variable |
| $\boldsymbol{x}$ | column vector |
| $\hat{\boldsymbol{x}}$ | column vector |
| $x_k$ | $k^{th}$ element of the column vector |
| $\mathbb{S}^2$ | unit sphere |
| $\langle f, g \rangle_{\mathbb{S}^2}$ | spherical inner product |
| $L^2(\mathbb{S}^2)$ | Hilbert space |
| $\mathcal{H}_L$ | band-limited Hilbert subspace |
| $\mathcal{H}_0$ | perfectly azimuthally symmetric Hilbert subspace |
| $\mathcal{H}_{LM}$ | order-limited Hilbert subspace |
| $Y_\ell^m$ | spherical harmonic basis of degree $\ell$ and order $m$ |
| $\mathbb{SO}(3)$ | rotation group |
| $\rho$ | collective denotation for all three Euler angles |
| $D^\ell_{m,m'}$ | Wigner-D basis |
| $d^\ell_{m,m'}$ | Wigner-d basis |
| $\lvert . \rvert$ | norm of the vector |
| $\overline{(.)}$ | complex conjugate |
| $(.)^T$ | vector transpose |
| $(.)^H$ | Hermitian |
| $\delta_{l,p}$ | Kronecker delta |

# Contents

# List of Figures

# List of Tables

# Chapter 1

# Introduction

## 1.1 Motivation and Background

Signal processing on spherical signals is a relatively new field of research that has become increasingly relevant in the past few years due to the prevalence of data sets defined on the sphere. These signals can range from the observable universe and celestial bodies to matter constituted of the smallest particles. In the past, signal processing techniques were designed for one-dimensional time domain or two-dimensional Euclidean domain signals, and mapping spherical signals to a two-dimensional plane had to be done in order to use these spherical methods. This approach, however, was problematic as it did not take into account the curvature of the sphere, leading to inaccurate computations. Consequently, there is a need for new signal processing methods that can accurately deal with data measured on a sphere.

Spherical signal processing is an integral part of numerous scientific and engineering disciplines, having seen an increase in attention and usage in the past two decades. It has been used to develop models and explain a variety of phenomena including and not limited to geodesy [1], geomagnetics, acoustics [2,3], computer graphics [4, 5], geophysics, computer vision, cosmology [6], medical imaging [7], astrophysics [8, 9], quantum chemistry [10], wireless communications [11,12] and 3D beamforming. A few examples manifesting applications of signal processing on the sphere are expanded on in this section.

Figure 1.1 shows climate data presented on NASA Science of Sphere global display system. NASA climate data on the sphere is a collection of data from NASA satellite observations that are used to understand the earth's climate and how it is changing. This data is used to study climate change and to inform climate models, which are used to make predictions about the future of the earth's climate. The

data is also used to measure air and ocean temperatures, water vapor concentrations, cloud cover, sea level, and other climate-related parameters. NASA also makes this data available to the public [13], allowing citizens to better understand the current state of the climate.

Figure 1.1: Climate data displayed on the NASA global display system

The cosmic microwave background (CMB) is a type of electromagnetic radiation believed to be left over from the Big Bang [14]. This radiation is an almost uniform background of light that permeates the entire universe. It has temperatures of around 2.7 Kelvin (-270.5°C) and is detected as microwaves. CMB radiation (as shown in Figure 1.2) is represented on the sphere as a pattern of tiny fluctuations in temperature. These fluctuations are believed to be the seeds of galaxies and other structures in the universe. The map [15, 16] of fluctuations is often depicted as a sphere that is filled with dark and light spots that correspond to the variations in temperature. This pattern is known as the Cosmic Microwave Background Radiation Anisotropy.

Cortical surface representation of the brain on the sphere [17] is a method of visualizing the brain in three dimensions. This method uses a sphere to represent the brain's surface, with the surface data mapped onto the sphere's surface. This method is used to understand the relationship between the brain's surface features, including sulci (folds) and gyri (ridges). This method also allows for a more detailed analysis of the brain's anatomy, as it can visualize even small features of the brain's surface. This method also allows for the study of brain connectivity and the neural pathways that connect different regions of the brain. Figure 1.3 shows

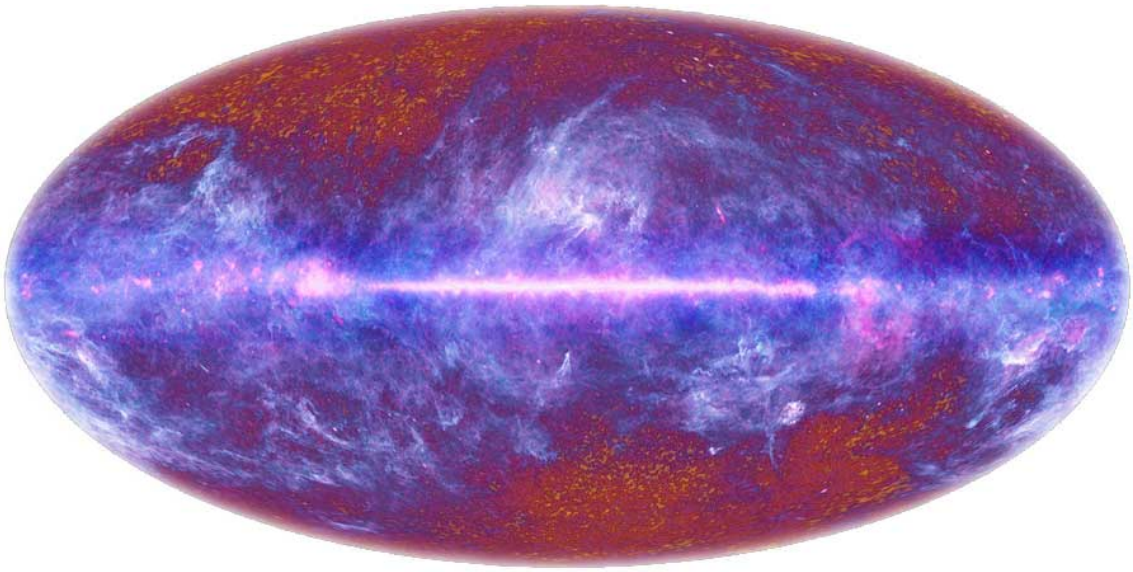

Figure 1.2: Cosmic microwave background radiation map

how cortical surface of the brain is interpolated using spherical maps.

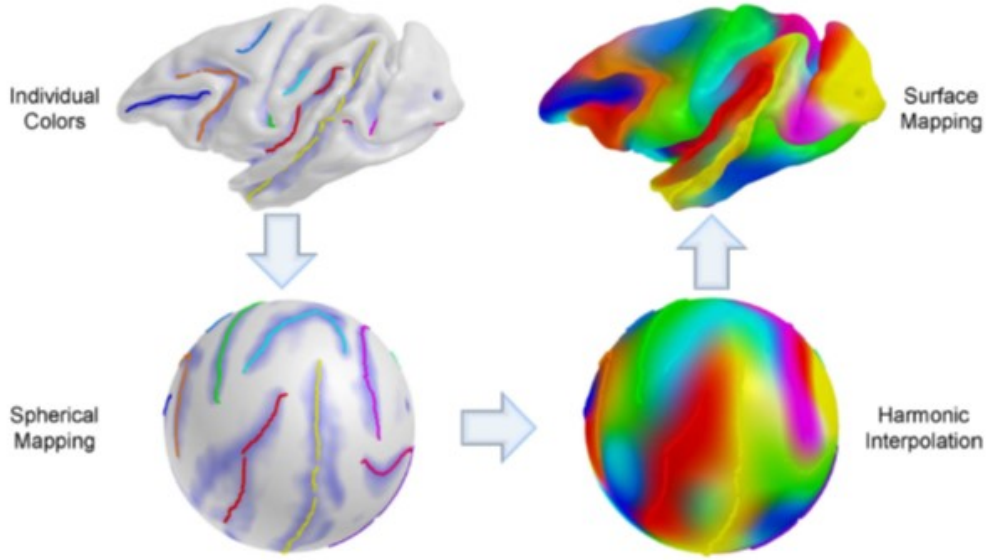


Figure 1.3: Cortical surface representation on the sphere

The head-related transfer function (HRTF) [18] is a mathematical representation that describes how sound signals bounce, scatter, and diffract when they reach the head, before travelling toward the ear canals. It is used in binaural sound representations on the sphere to simulate the way sound is perceived in the real world. This representation can then be used to create realistic 3D soundscapes in virtual reality and other applications. Figure 1.4 shows the data collection process at the Wright-Patterson Air Force Base [19] in Dayton, Ohio.

Figure 1.4: HRTF data collection at the Wright-Patterson Air Force Base

## 1.2 Literature Review

A sampling scheme defines which points on a spherical manifold are to be measured in order to obtain data in the spatial domain. The spherical harmonic transform (SHT) is a tool that casts the spatial representation of a spherical signal to the spectral domain. It is an analogue of the Fourier transform for spherical signals. In order to carry out analysis in the harmonic domain, a computationally efficient sampling strategy is needed in order to minimize the number of samples needed to accurately obtain the SHT of a signal. Several different methods for sampling band-limited signals on the sphere – leading to accurate computation of the SHT – have been documented [16, 20–32]. Each sampling scheme requires a distinct number of sampling points in a unique configuration to accurately represent the information contained within band-limited signals.

Iso-latitude sampling schemes, where samples along longitude are taken over equi-spaced latitudinal rings, permit computation of SHT via separation of variables, which significantly reduces the computational complexity. Existing schemes either require $4L^2$, $2L^2$ or $L^2$ number of samples. Driscoll and Healy [22] developed a method for accurate SHTs of signals band-limited to $L$, which involves taking $\sim 4L^2$ equiangular samples on the sphere. This was done by dividing the sphere into $2L-1$ latitude rings and assigning $2L-1$ samples to each one. In comparison, McEwen and Wiaux's (MW) sampling scheme [27] requires $\sim 2L^2$ equiangular samples in order to obtain an exact calculation of the SHT. The Gauss-Legendre (GL) sampling method also requires a $\sim 2L^2$ grid to exactly compute the SHT [27, 33]. The time complexity of the SHTs of these sampling methods is of order $O(L^3)$. As far as we know, no sampling scheme of dimensionality less than $\sim 2L^2$ has been developed.

A new sampling configuration, called the Optimal Dimensionality (OD) sampling scheme, was proposed by Khalid et. al. [20] which takes $2L^2$ optimal number of samples as a means of accurately computing the SHT and ISHT of band-limited signals. Applications in diffusion MRI [21] and acoustics [34] have enhanced their experience by utilizing the OD sampling scheme. Although this sampling scheme is spatially economical, its associated SHT has a computational complexity of order $O(L^4)$ due to the sequence of matrix inversions required for its computation.

Two additional sampling schemes that can be used to approximate the SHT are the HEALPix (Hierarchical Equal Area iso-Latitude Pixelization of a sphere) [24] and IGLOO [31] schemes. HEALPix pixelizes the spherical surface into equal-area partitions, each with its center located on latitudinally constant discrete rings. The IGLOO scheme also partitions the sphere in the same manner, centred on iso-latitude rings that enable a fast transform via variable separation. Other sampling methods include the scheme devised by Sneeuw [23], which despite needing $L^2$ number of samples, becomes precisionally unreliable for high band-limits.

A signal has azimuthal symmetry, if there exists an axis of rotation (usually called the $z$ axis), such that the signal doesn't change if you rotate it by an angle $0 \leq \phi \leq 2\pi$ around that axis. Nearly azimuthally symmetric (NAS) signals are a class of azimuthally symmetric (AS) signals that exhibit a nearly uniform behavior throughout the entire latitudinal great circle. In other words, there is very little variation in the signal values throughout the sample space on each vertical axial gradation (iso-latitude or otherwise). Applications that utilize NAS signals (e.g. radar beam patterns) require computation of all spherical coefficients in conventional approaches. In this study, we demonstrate the advantage of computing only

an effective set of coefficients by exploiting the redundant propensity of certain coefficients. In addition to that, some applications make use of high level of azimuthal symmetry for reduced number of sample acquisition, such as in antenna radiation patterns [35]. However, any degradation in the axial symmetry results in unwanted modeling errors. Thus, it is important to formulate a framework for accurate representation of such NAS signals. There is extensive literature on spherical sampling schemes as well as accurate and efficient band-limited SHT computation methods. However, in this work, we demonstrate the utility of order-limiting band-limited signals that are NAS.

# Chapter 2

# Mathematical Preliminaries and Problem Under Consideration

We look at the spherical coordinate system and other mathematical formulae necessary for signal processing in the spherical domain.

## 2.1 Unit Sphere

Any location in the Euclidean space can be described by

$$\boldsymbol{x} \equiv (x_x, x_y, x_z)^T \in \mathbb{R}^3. \tag{2.1}$$

Here, $(.)^T$ represents the vector transpose. The planar and vertical axes components of the vector $\boldsymbol{x}$ are denoted by $x_x$, $x_y$ and $x_z$. Strength of the vector $\boldsymbol{x}$ is defined as

$$\boldsymbol{x} = \sqrt{x_x^2 + x_y^2 + x_z^2}. \tag{2.2}$$

The unit sphere is a collection of points on a spherical surface in a three-dimensional space. It is mathematically represented as

$$\mathbb{S}^2 = \{\boldsymbol{x} \in \mathbb{R}^3 : |\boldsymbol{x}| = 1\}. \tag{2.3}$$

Unit vectors representing points on the sphere have a magnitude of one. All vectors have their accompanying unit vectors. The unit vector $\hat{\boldsymbol{x}}$ is a scaled version of the original vector with a magnitude of one. It is defined as

$$\hat{\boldsymbol{x}} = \frac{\boldsymbol{x}}{|\boldsymbol{x}|}, \tag{2.4}$$

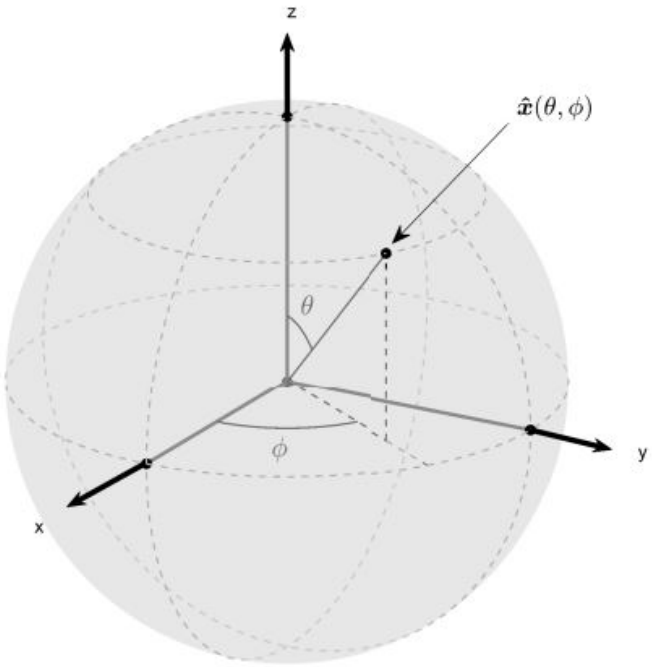


Figure 2.1: Spherical coordinates at point $\hat{\boldsymbol{x}}(\theta, \phi)$

The size and direction of a vector $\boldsymbol{x}$ can be described by $|\boldsymbol{x}|$ and $\hat{\boldsymbol{x}}$ respectively. Therefore, the spherical surface can be reinterpreted as $\mathbb{S}^2 = \{\hat{\boldsymbol{x}} \in \mathbb{R}^3\}$.

### 2.1.1 The Spherical Coordinate System

Any point on a spherical surface can be represented by the co-latitude (or elevation) and longitude (or azimuth). The former is denoted by $\theta \in [0, \pi]$ and measured from the positive z-axis; the latter is represented as $\phi \in [0, 2\pi]$ and valuated from the positive x-axis in the x-y plane. Every point on the spherical surface can be described by a unit vector parameterized by the co-latitude and longitude as

$$\hat{\boldsymbol{x}} \equiv \hat{\boldsymbol{x}}(\theta, \phi) \triangleq (\sin\theta\cos\phi, \sin\theta\sin\phi, \cos\theta)^T. \tag{2.5}$$

The azimuth and elevation can be calculated from the given unit vector on the sphere as

$$\theta = \cos^{-1} x_z, \;\; \phi = \tan^{-1}\left(\frac{x_y}{x_x}\right), \tag{2.6}$$

where $\tan^{-1}$ is assumed to be operational in the four quadrants.

### 2.1.2 Rotations on the Sphere

There are two types of rotational systems: intrinsic and extrinsic. An intrinsic system is one in which rotations are performed on the coordinate system rotated by the previous operation(s). In an extrinsic system, rotations are performed on the signal while the coordinate system stays static. Of the 24 axial permutations in total, the $zyz$ convention is the one most widely used. It defines a rotation using $\varphi \in [0, 2\pi)$ about the $z$-axis, $\vartheta \in [0, \pi]$ about the $y$-axis, and $\omega \in [0, 2\pi)$ about the $z$-axis. Each rotation is represented by a $3 \times 3$ orthogonal matrix. The complete rotation is defined as

$$\mathbf{R} \equiv \mathbf{R}^{zyz}(\varphi, \vartheta, \omega) \triangleq \mathbf{R}^{z}(\varphi)\mathbf{R}^{y}(\vartheta)\mathbf{R}^{z}(\omega), \tag{2.7}$$

where $\mathbf{R}^{z}(\varphi)$, $\mathbf{R}^{y}(\vartheta)$ and $\mathbf{R}^{z}(\omega)$ are the 3 x 3 orthogonal matrices standing for rotations around $z$, $y$ and $z$ axes respectively. They are defined as

$$\mathbf{R}^{z}(\varphi) = \begin{pmatrix} \cos\varphi & -\sin\varphi & 0 \\ \sin\varphi & \cos\varphi & 0 \\ 0 & 0 & 1 \end{pmatrix}, \ \mathbf{R}^{y}(\vartheta) = \begin{pmatrix} \cos\vartheta & 0 & \sin\vartheta \\ 0 & 1 & 0 \\ -\sin\vartheta & 0 & \cos\vartheta \end{pmatrix}. \tag{2.8}$$

The third orthogonal matrix $\mathbf{R}^{z}(\omega)$ is the same as $\mathbf{R}^{z}(\varphi)$ with a different variable.

## 2.2 Spherical Signal Analysis

Spatial spherical signals of the form $f(\theta, \phi) \equiv f(\hat{\boldsymbol{x}})$ can have complex values and are square integrable. They are defined on the spherical surface as

$$||f||_{\mathbb{S}^2} = \sqrt{\int_{\mathbb{S}^2} |f(\hat{\boldsymbol{x}})|^2 ds(\hat{\boldsymbol{x}})} \ < \infty, \tag{2.9}$$

where the whole sphere is integrated and $ds(\hat{\boldsymbol{x}})$ is the invariant measure on the sphere. The double integration over the sphere is parameterized by the latitude and longitude as

$$\int_{\mathbb{S}^2} \equiv \int_{\phi=0}^{2\pi} \int_{\theta=0}^{\pi}. \tag{2.10}$$

The inter-function inner product is defined as

$$\langle f, g \rangle_{\mathbb{S}^2} \triangleq \int_{\mathbb{S}^2} f(\hat{\boldsymbol{x}}) \overline{h(\hat{\boldsymbol{x}})} ds(\hat{\boldsymbol{x}}), \tag{2.11}$$

where $\overline{(.)}$ stands for the complex conjugate, and the set of functions spans the Hilbert space in $L^2(\mathbb{S}^2)$. Induced by the inner product in (2.11), the strength of the function in (2.9) is given by $\langle f, f \rangle_{\mathbb{S}^2}$. Signals on the sphere are always finite energy functions.

### 2.2.1 Spherical Harmonic Basis Functions

We use orthogonal Hilbert space $L^2(\mathbb{S}^2)$ basis functions to map the spherical signal into the harmonic domain, in order that spectral domain analysis can be carried out on the spatial domain spherical signal. The spherical harmonic basis (SHB) functions are denoted by $Y_\ell^m(\theta, \phi)$ and defined as

$$Y_\ell^m(\theta, \phi) = \sqrt{\frac{2\ell + 1}{4\pi} \frac{(\ell - m)!}{(\ell + m)!}} P_\ell^m(\cos\theta) e^{im\phi}, \tag{2.12}$$

where $\ell \geq 0$ is the degree number, $-\ell \leq m \leq \ell$ is the order number, and $P_\ell^m(.)$ is the canonical Legendre polynomial [36]. SHB functions are orthonormal in nature, i.e.

$$\langle Y_\ell^m, Y_{\ell'}^{m'} \rangle \triangleq \int_{\mathbb{S}^2} Y_\ell^m(\theta, \phi) Y_{\ell'}^{m'}(\theta, \phi) \sin\theta d\theta d\phi = \delta_{\ell\ell'} \delta_{mm'}, \tag{2.13}$$

where $\delta_{\ell\ell'}$ stands for the Kronecker delta function. The conjugation property of SHB functions is defined as

$$\overline{Y_\ell^m(\theta, \phi)} = (-1)^m Y_\ell^{-m}(\theta, \phi). \tag{2.14}$$

Table 2.1 shows some examples of SHB functions for the first four degrees $\ell = 0, 1, 2, 3$ and their corresponding orders $-\ell \leq m \leq \ell$.

### 2.2.2 Spherical Harmonic Transform

Since the spherical harmonics basis functions span the Hilbert space $L^2(\mathbb{S}^2)$, any spherical function $f \in L^2(\mathbb{S}^2)$ can be stored as a synthetic combination of the SHB functions, i.e.

$$f(\theta, \phi) = \sum_{\ell=0}^{\infty} \sum_{m=-\ell}^{\ell} (f)_\ell^m Y_\ell^m(\theta, \phi), \tag{2.15}$$

where $(f)_\ell^m$ is the harmonic coefficient (factor) of degree $\ell$ and order $m$. It can be computed by the spherical harmonic transform (SHT) as

Table 2.1: Spherical Harmonic Basis Functions

| **Degree**, $\ell$ | **Order**, $m$ | $Y_\ell^m(\theta,\phi)$ |
|---|---|---|
| 0 | 0 | $\frac{1}{2}\sqrt{\frac{1}{\pi}}$ |
| 1 | -1 | $\frac{1}{2}\sqrt{\frac{3}{2\pi}}e^{-i\phi}\sin\theta$ |
| 1 | 0 | $\frac{1}{2}\sqrt{\frac{3}{\pi}}\cos\theta$ |
| 1 | 1 | $\frac{-1}{2}\sqrt{\frac{3}{2\pi}}e^{i\phi}\sin\theta$ |
| 2 | -2 | $\frac{1}{4}\sqrt{\frac{15}{2\pi}}e^{-2i\phi}\sin^2\theta$ |
| 2 | -1 | $\frac{1}{2}\sqrt{\frac{15}{2\pi}}e^{-i\phi}\sin\theta\cos\theta$ |
| 2 | 0 | $\frac{1}{4}\sqrt{\frac{5}{\pi}}(3\cos^2\theta-1)$ |
| 2 | 1 | $\frac{-1}{2}\sqrt{\frac{15}{\pi}}e^{i\phi}\sin\theta\cos\theta$ |
| 2 | 2 | $\frac{1}{4}\sqrt{\frac{15}{2\pi}}e^{2i\phi}\sin^2\theta$ |
| 3 | -3 | $\frac{1}{8}\sqrt{\frac{35}{\pi}}e^{-3i\phi}\sin^3\theta$ |
| 3 | -2 | $\frac{1}{4}\sqrt{\frac{105}{2\pi}}e^{-2i\phi}\sin^2\theta\cos\theta$ |
| 3 | -1 | $\frac{1}{8}\sqrt{\frac{21}{\pi}}e^{-i\phi}\sin\theta(5\cos^2\theta-1)$ |
| 3 | 0 | $\frac{1}{4}\sqrt{\frac{7}{\pi}}(5\cos^3\theta-3\cos\theta)$ |
| 3 | 1 | $\frac{-1}{8}\sqrt{\frac{21}{\pi}}e^{i\phi}\sin\theta(5\cos^2\theta-1)$ |
| 3 | 2 | $\frac{1}{4}\sqrt{\frac{105}{2\pi}}e^{2i\phi}\sin^2\theta\cos\theta$ |
| 3 | 3 | $\frac{-1}{8}\sqrt{\frac{35}{2\pi}}e^{3i\phi}\sin^3\theta$ |

$$(f)_\ell^m \triangleq \langle f, Y_\ell^m\rangle = \int_{\mathbb{S}^2} f(\theta,\phi)\ \overline{Y_\ell^m(\theta,\phi)}\sin\theta d\theta d\phi. \tag{2.16}$$

Equation (2.15) is used to recover a signal from its harmonic coefficients. It is interchangeably referred to as the synthesis equation and the Inverse Spherical Harmonic Transform (ISHT). On the other hand, the forward SHT is given by the analysis equation in (2.16).

### 2.2.3 Band-limited Signals on the Sphere

A spherical signal $f \in L^2(\mathbb{S}^2)$ is called band-limited to degree $L$ if $(f)_\ell^m = 0$ for $\ell \geq L$ and $|m| \leq \ell$. The collection of all such band-limited spherical signals forms an $L^2$ dimensional subspace of the Hilbert Space $L^2(\mathbb{S}^2)$. This band-limited space is represented by $\mathcal{H}_L$ and defined as

$$\mathcal{H}_L \triangleq \{f \in L^2(\mathbb{S}^2) : (f)_\ell^m = 0,\ \forall\ \ell \geq L, |m| \leq L\}. \tag{2.17}$$

For a bandlimited spherical signal $f \in \mathcal{H}_L$, the summation for all degree numbers in (2.15) is cut off at $L-1$, i.e.

$$f(\theta, \phi) = \sum_{\ell=0}^{L-1} \sum_{m=-\ell}^{\ell} (f)_\ell^m Y_\ell^m(\theta, \phi), \tag{2.18}$$

and the harmonic factors are represented by an $L^2$ x 1 vector as

$$\mathbf{f} = \left[\ (f)_0^0,\ (f)_1^{-1},\ (f)_1^0,\ (f)_1^1,\ \dots\ ,\ (f)_{(L-1)}^{(L-1)}\ \right]^\top. \tag{2.19}$$

Any value in the spectral coefficient vector can be accessed using the following indexing scheme:

$$n \triangleq \ell(\ell+1) + m,\ \ell = \lfloor\sqrt{n}\rfloor, m = n - \lfloor\sqrt{n}\rfloor(\lfloor\sqrt{n}\rfloor + 1), \tag{2.20}$$

where $n$ is the position of the coefficient described by degree $\ell$ and order $m$, and $\lfloor . \rfloor$ is the integer floor function. Hence, $(f)_\ell^m \equiv (f)_n$, where $n = 0, 1, ..., L^2 - 1$. The coefficients get smaller as the band-limit increases.

### 2.2.4 Sampling Schemes on the Sphere

Let us look at existing spherical sampling schemes which allow accurate recovery of band-limited signals. The number of samples needed to accurately compute an SHT of a spherical signal limited to $L$ bands is referred to as the spatial dimensionality. This number will be denoted by $N$.

#### 2.2.4.1 Gauss-Legendre Quadradrature Sampling

Because it is based on the Gauss-Legendre (GL) quadrature on the sphere [16], this sampling scheme is called the Gauss-Legendre sampling scheme. The GL Quadrature can be used to develop a sampling theorem that allows for an exact calculation of the SHT of a signal that is limited by a certain frequency band. This

scheme requires a total of $N_{GL} = L(2L-1)$ number of samples to precisely compute an SHT for a signal limited to $L$ bands. These samples are taken from $L$ equispaced latitude rings with $2L-1$ equiangular samples along the longitude $\phi$. The ring placement along the co-latitude $\theta$ is determined by the Legendre polynomial roots of order $L$, as determined by the GL quadrature, which is used to break down the integral given in (2.16) into discrete parts. Other versions of the GL quadrature scheme that required fewer sampling points have also been documented [37].

#### 2.2.4.2 Equiangular Sampling

Driscoll and Healy [22] proposed an equiangular sampling method for signals band-limited to $L$. This scheme has a requirement of $2L$ number of iso-latitude rings with the same number of longitudinal samples in each ring. McEwen et. al. [27], developed an equiangular scheme that samples at specific, predetermined points arranged in an equiangular grid. The positions are described by the following definitions:

$$\theta_i = \frac{\pi(2i+1)}{2L-1}, \quad i = 0, 1, 2, ..., L-1, \tag{2.21}$$

$$\phi_j = \frac{2\pi j}{2L-1}, \quad j = 0, 1, 2, ..., 2L-2. \tag{2.22}$$

This method halves the number of equiangular samples required for precise computation of SHT. It requires one sample at either of the poles ($\theta = 0$ or $\theta = \pi$) and $L-1$ equiangular rings with $2L-1$ longitudinal samples. It has a spatial dimensionality of $N_E = (L-1)(2L-1)+1$ samples, which is an improvement on the GL sampling scheme by $3(L-1)$.

#### 2.2.4.3 Optimal Dimensionality Sampling

A novel sampling scheme that requires a set of $L^2$ points has been developed by Khalid et. al. [20] to accurately perform the SHT on signals that are band-limited to $L$. For an $L$ degree band-limited signal, the ideal spatial dimensionality is $\mathcal{H}_L$, which is what the writers of [20] achieved in their proposed sampling configuration. The sampling scheme boasts reasonable reconstruction errors for band-limits as high as $L = 2048$. Like other iso-latitude sampling schemes, the $\theta$ space is segmented into equiangular rings. Let $\theta_k$, for $k$ ranging from 0 to $L-1$, be the latitudinal sampling positions. For a ring placed at $\theta_k$, the positions of the $\phi$ samples are given by

$$\phi_n^k = \frac{2\pi n}{2k+1}, \quad n = 0, 1, ..., 2k. \tag{2.23}$$

The following expression quantifies the spatial dimensionality of this scheme:

$$N_O = \sum_{k=0}^{L-1}(2k+1) = L^2. \tag{2.24}$$

### 2.2.5 Axis-symmetric Signals on the Sphere

An axis-symmetric or azimuthally symmetric (AS) signal is one in which there is no dependence on the longitude, i.e. $f(\theta, \phi) = f(\theta)$. All such signals are classified under and denoted by $\mathcal{H}_0$. This subspace of the Hilbert Space $L^2(\mathbb{S}^2)$ is defined as

$$\mathcal{H}_0 \triangleq \{f \in L^2(\mathbb{S}^2) : f(\theta, \phi) = f(\theta)\}. \tag{2.25}$$

From the synthesis equation in (2.15), for any signal $f \in \mathcal{H}_0$, $(f)_l^m = 0$ for $m \neq 0$,

$$f(\theta, \phi) = \sum_{\ell=0}^{L-1} (f)_\ell^0 \; Y_\ell^0(\theta, \phi). \tag{2.26}$$

## 2.3 Spherical Harmonic Parseval Relation

Using Parseval's theorem, the harmonic factors can be used to determine the total energy of a spherical function $f \in \mathbb{S}^2$ as

$$||f||^2 = \int_{\mathbb{S}^2} |f(\hat{\boldsymbol{u}})|^2 ds(\hat{\boldsymbol{u}}) = \langle f, f \rangle, \tag{2.27}$$

where

$$\langle f, f \rangle = \sum_{\ell,m} |(f)_m^\ell|^2 \tag{2.28}$$

holds due to the orthonormality property of spherical harmonics.

## 2.4 Wigner-D Functions

The rotational Hilbert Space $L^2(\mathbb{SO}(3))$, like its static counterpart, has a complete set of orthogonal bases. They are called the Wigner-D functions and defined as

$$D_{m,m'}^\ell(\rho) \triangleq e^{-im\phi} \; d_{m,m'}^\ell(\vartheta) \; e^{-im\omega}, \;\; \rho \equiv (\varphi, \vartheta, \omega), \tag{2.29}$$

where $d^{\ell}_{m,m'}(\vartheta)$ are the Wigner-d functions of degree $\ell > 0$ and orders $m \leq \ell, m \leq \ell'$. Wigner-d functions conform to the following orthogonality property:

$$\int_0^{\pi} d^{\ell}_{m,m'}(\vartheta) d^{p}_{m,m'}(\vartheta) \sin\vartheta d\vartheta = \frac{2}{(2\ell+1)} \delta_{\ell,p}. \tag{2.30}$$

Because the Wigner-D functions are complete in the rotational Hilbert Space, any rotational spherical signal $f \in L^2(\mathbb{SO}(3))$ can be synthesised as

$$f(\rho) = \sum_{\ell=0}^{\infty} \sum_{m=-\ell}^{\ell} \sum_{m'=-\ell}^{\ell} (f)^{\ell}_{m,m'} D^{\ell}_{m,m'}(\rho), \tag{2.31}$$

where

$$(f)^{\ell}_{m,m'} \triangleq \left(\frac{2\ell+1}{8\pi^2}\right) \int_{\mathbb{SO}(3)} f(\rho) \overline{D^{\ell}_{m,m'}(\rho)}\, d\rho \tag{2.32}$$

is the rotational spectral coefficient of degree $\ell$ and orders $m, m'$.

## 2.5 Problem Identification

Representing spherical signals that are NAS using existing sampling schemes leads to wasteful computations as signal dependence on higher orders for such signals becomes increasingly negligible. By exploiting order-limiting potential in existing sampling schemes, unnecessary computations can be avoided while maintaining accuracy in signal representation. This computational saving needs to be demonstrated on two distinct sampling schemes in light of an application in antenna theory.

# Chapter 3

# Order-limiting Gauss-Legendre Quadrature Samples

Spherical signal processing includes signal processing in spatial and spectral domains that are linked to each other via the well-known spherical harmonic transform (SHT) [22, 27, 36]. Since datasets may be very large [2], sample acquisition on the sphere must necessitate the least number of spherical samples for precise computation of SHT. This study investigates the advantages of computing a subset of spherical coefficients instead of all coefficients for applications that make use of signals that are nearly azimuthally symmetric (NAS). This is particularly useful for antenna radiation patterns [35], as any degradation in the axial symmetry can lead to modeling errors. We propose a framework for accurate representation of such signals by order-limiting the band-limited signals. Although there is literature on spherical sampling schemes and efficient computation of the SHT [20, 22–27, 29, 31, 32], we demonstrate the utility of order-limiting for NAS signals using the Gauss Legendre (GL) Quadrature sampling scheme.

## 3.1 The Sampling Scheme

We consider a problem to design a method – using the GL Quadrature sampling scheme – for the sampling of order-limited signals such that SHT of the signal can be computed accurately and efficiently. To the best of our knowledge, none of the existing sampling techniques exploit the order-limiting potential of an NAS signal to reduce the number of samples without compromising the accuracy of associated SHT.

### 3.1.1 Harmonic Formulation

A signal $L^2(\mathbb{S}^2)$ exhibits azimuthal symmetry if $f(\theta,\phi) = f(\theta)$. Azimuthally symmetric (AS) signals – a special form of rotationally symmetric signals with z-axis as axis of rotation – form a subspace denoted by $\mathcal{H}_0 \subseteq L^2(\mathbb{S}^2)$. For $f \in \mathcal{H}_0$, $(f)_l^m = 0$ for $m \neq 0$, which implies that an AS signal is expanded using zero-order spherical harmonics.

A signal $f \in L^2(\mathbb{S}^2)$ is band-limited to degree $L$ when $(f)_\ell^m = 0, \forall\ \ell \geq L$. Such band-limited signals form an $L^2$ dimensional subspace denoted by $\mathcal{H}_L \subseteq L^2(\mathbb{S}^2)$. Furthermore, a signal $f \in \mathcal{H}_L$ is considered to be order-limited to $M < L$ if $(f)_\ell^m = 0\ \forall\ \ell \geq L, m > M$, and therefore can be represented as

$$f(\theta,\phi) = \sum_{\ell=0}^{L-1} \sum_{m=-N}^{N} (f)_\ell^m Y_\ell^m(\theta,\phi), \quad N = \min(\ell, M). \tag{3.1}$$

The signals of the form given in (3.1) make $M^2+(L-M)(2M+1)$ subspace denoted by $\mathcal{H}_{LM} \subseteq \mathcal{H}_L$. It follows that $\mathcal{H}_{LM} \subset \mathcal{H}_L\ \forall\ M < L$. By expressing the spherical harmonic basis function of degree $\ell$ and order $m$ as

$$Y_\ell^m(\theta,\phi) = \widetilde{Y}_\ell^m(\theta) e^{-im\phi}, \tag{3.2}$$

and defining $F_m(\theta)$ as

$$F_m(\theta) = \int_{\phi=0}^{2\pi} f(\theta,\phi) e^{-im\phi}, \tag{3.3}$$

we reformulate SHT given in (2.16) as

$$(f)_\ell^m = \int_{\theta=0}^{\pi} F_m(\theta) \widetilde{Y}_\ell^m(\theta) \sin\theta d\theta, \tag{3.4}$$

We can use (3.3) and (3.4) to compute SHT, provided the integrals can be discretized and evaluated accurately.

### 3.1.2 Proposed Sampling Scheme and Spherical Harmonic Transform

We present an iso-latitude sampling method that takes $L$ equi-spaced rings with $2M+1$ equiangular samples along longitude ($\phi$). Using the representation of order-limited signals in (3.1) and exploiting the orthogonality of complex exponentials, we can also express $F_m(\theta)$ in (3.3) as

$$F_m(\theta) = 2\pi \sum_{\ell=|m|}^{L-1} (f)_\ell^m \widetilde{Y}_\ell^m(\theta), \quad |m| \leq M, \tag{3.5}$$

using which the signal $f(\theta, \phi)$ can be expanded as

$$f(\theta, \phi) = \frac{1}{2\pi} \sum_{m=-M}^{M} F_m(\theta) e^{im\phi}, \tag{3.6}$$

which indicates that $f(\theta, \phi)$ can be recovered from $F_m(\theta)$ if we take at least $2M+1$ samples along $\phi$ for each $\theta$. Since the formulation in (3.5) indicates that $F_m(\theta)$ is an $L-1$ degree polynomial, the integrand in (3.6) is of maximum degree $2L-1$. We can therefore evaluate an integral in (3.6) using GL quadrature as

$$(f)_\ell^m = \sum_{i=0}^{L-1} G_m(\theta_i) \widetilde{Y}_\ell^m(\theta_i) w_i, \tag{3.7}$$

where $\theta_i \; \forall \; i = 1, 2, \ldots, L$ are co-latitude samples taken as roots of the Legendre polynomial of degree $L$, and $w_i$ denotes GL quadrature weight associated with $\theta_i$. The proposed SHT is computed by Algorithm 1 shown below.

**Algorithm 1** Forward SHT

**Require:** $(f)_\ell^m \; \forall \; 0 \leq \ell \leq (L-1), |m| \leq min(\ell, M)$

1: **procedure** FORWARD-SHT($f(\theta, \phi)$)
2: initialize $(f)_\ell^m$ vector of size $M^2 + (L-M)(2M+1)$
3: **for** $\ell = 0, 1, ..., L-1$ iterations **do**
4: **for** $m = min(\ell, M)$ **do**
5: compute $G_m(\theta)$ by taking $2M+1$ point FFT
6: sum the product $G_m(\theta_i) \widetilde{Y}_\ell^m(\theta_i) w_i$ for $L$ rings
7: **end for**
8: **end for**
9: **end procedure**

The synthesis procedure is characterized by equations (3.5) and (3.6). The proposed ISHT is shown in Algorithm 2 below.

### 3.1.3 Numerical Accuracy Analysis

To analyse the accuracy of the transforms, we generate a band-limited and order-limited signal $f_{\text{BOL}} \in \mathcal{H}_{LM}$ by randomly initializing complex numbers of unity magnitude as its harmonic factors $(f_{\text{BOL}})_\ell^m$ for $0 < \ell < L, |m| \leq \min(\ell, M)$. We synthesize the spatial signal by inverse SHT for $4 \leq L \leq 1024$ and $M = L/2$. This is followed by a forward transform to obtain reconstructed harmonic factors

**Algorithm 2** Inverse SHT

**Require:** $f(\theta, \phi)$

**procedure** INVERSE-SHT($(f)_l^m$)
  initialize $f(\theta, \phi)$ vector of size $L(2M+1)$
  **for** $\ell = 0, 1, ..., L-1$ iterations **do**
    **for** $m = min(\ell, M)$ **do**
      compute dot product $(f)_l^m \ \widetilde{Y}_\ell^m$ for $L$ rings
    **end for**
    get $f(\theta, \phi)$ by taking $(2M+1)$ point ifft
  **end for**
**end procedure**

referred to as $(f_r)_\ell^m$. This is repeated ten times to record the average value for the mean and maximum errors $E_{\text{mean}}$ and $E_{\max}$ given by

$$E_{\text{mean}} = \frac{1}{L^2} \sum_{\ell=0}^{L-1} \sum_{m=-\min(\ell,M)}^{\min(\ell,M)} \left| (f_{\text{BOL}})_\ell^m - (f_r)_\ell^m \right|, \tag{3.8}$$

$$E_{\max} = \max \left| (f_{\text{BOL}})_\ell^m - (f_r)_\ell^m \right|, \tag{3.9}$$

which are plotted in Fig. 3.1. We also plot the reconstruction error $|(f_{\text{BOL}})_\ell^m - (f_r)_\ell^m|$ for one realization, $L = 1024$ and $M = 256$ on a base-10 logarithmic scale in Fig. 3.2. These plots indicate that the proposed order-limited GL sampling method and its SHTs allow signal reconstruction with negligible errors.

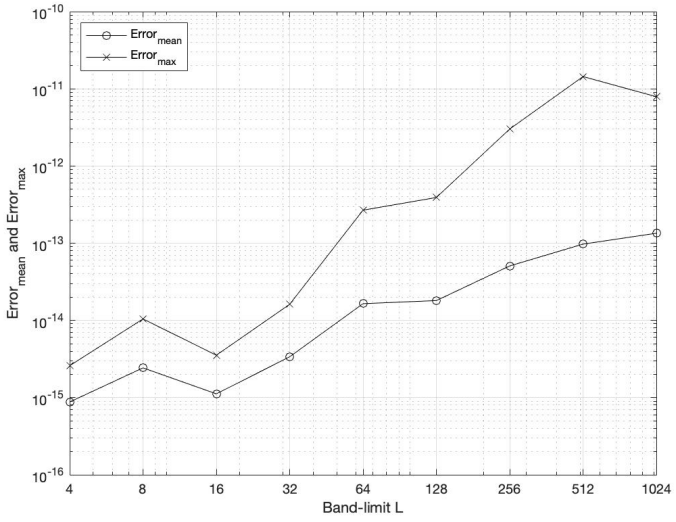


Figure 3.1: Mean and maximum reconstruction errors (GL)

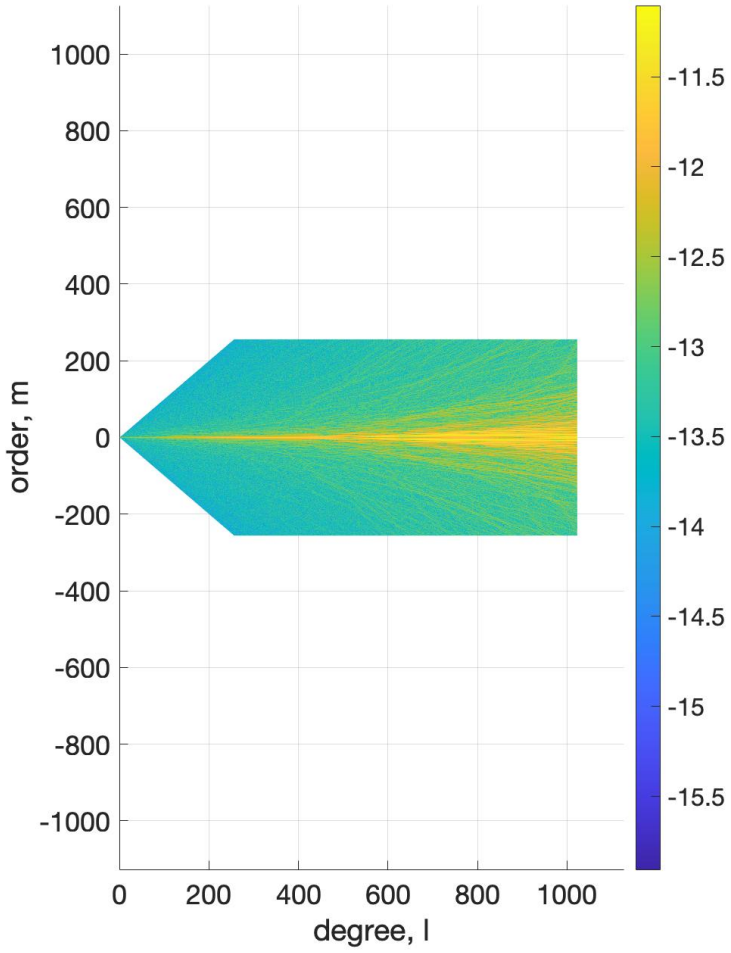


Figure 3.2: Reconstruction error for $L = 1024$, $M = 256$ (GL)

### 3.1.4 Computational Complexity

The time required to compute the proposed transforms for order-limited signals are shown in Fig. 3.3. These are plotted for band-limits $4 \leq L \leq 1024$ while limiting the order at $L/2 \,\forall\, L$. The times are averaged over 10 random signals and measured in MATLAB running on a laptop computer equipped with 2.7 GHz Intel Core i5 processor with 8 GB RAM. The experimental times for the transforms evolve with the band-limit as $O\left(L\left(M^2 + (L-M)(2M+1)\right)\right)$ – which is the theoretical computational complexity of the proposed transforms – increases linearly with the band-limit. We note that the complexity of the proposed transforms is less than the complexity $O\left(L^3\right)$ of the SHTs associated with the sampling methods that do not exploit the order-limiting potential of a signal.

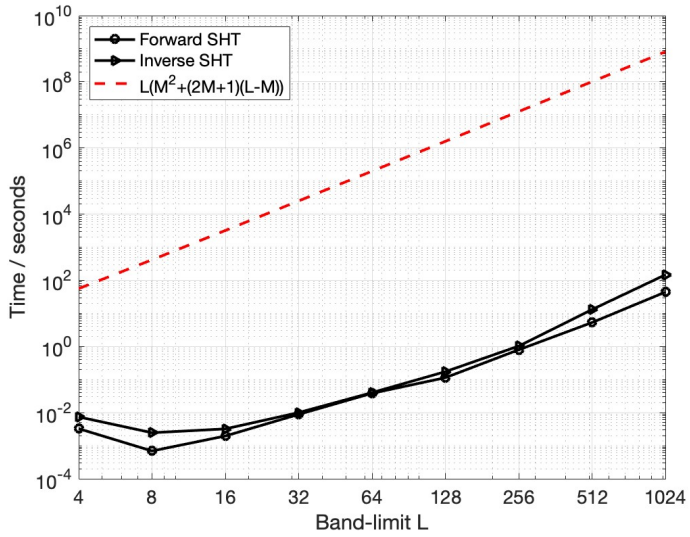


Figure 3.3: Time complexity analysis of forward and inverse transforms (GL)

## 3.2 Application: Sampling Antenna Radiation Pattern

We consider a dipole antenna radiation pattern with perfect azimuthal symmetry defined in [38] as

$$r(\theta,\phi) = \left| \frac{\cos(kY\cos(\theta)/2) - \cos(kY/2)}{\sin(\theta)} \right|^2, \tag{3.10}$$

where $k$ is the phase constant and $Y$ is the antenna length. Here, $k$ and $Y$ are taken as $\frac{2\pi}{\lambda}$ and $1.4\lambda$ respectively, where $\lambda$ is the wavelength taken to be 1.0 m. We introduce random rotational perturbations to model the fact that the radiation pattern is not perfectly AS in practice, that is,

$$\tilde{r}(\theta,\phi) = \frac{1}{P}\sum_{i=1}^{P} D\left(\alpha_i,\beta_i\right) r(\theta,\phi), \tag{3.11}$$

where $D(\alpha,\beta)$ is a Wigner-D like operator that rotates the signal by $\beta$ around $y$-axis followed by an $\alpha$ rotation around $z$-axis. We choose both $\alpha_i, \beta_i$ uniformly distributed in $[0,\pi/6]$ for $P = 10$ rotations to corrupt the perfectly AS signal, thus rendering it NAS. The radiation pattern $\tilde{r}(\theta,\phi)$ is plotted in spatial and spectral domains in Fig. 3.4 and Fig. 3.5 respectively.

In order to find the band-limit of the perturbed signal, we analyze the reconstruction error, plotted in Fig. 3.6, for different bandlimits and choose $L = 28$ as an effective band-limit of the signal. In order to find order-limit of the signal, we take

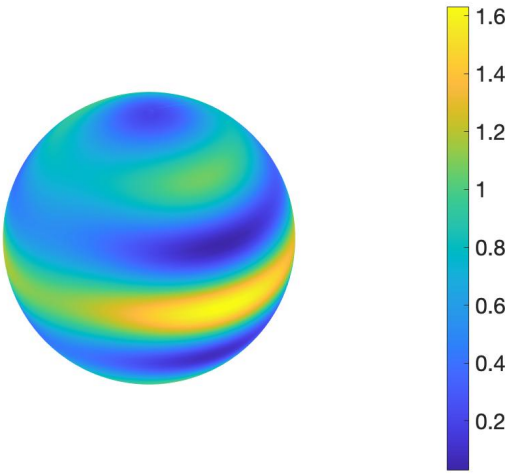


Figure 3.4: Antenna radiation pattern in the spatial domain (GL)

the ratio of energies of spectral coefficients of the order and band-limited signal with respect to the band-limited signal only, so as to gauge the significant loss of energy when reducing the order-limit of the signal. Upon reducing the order of the signal, this energy ratio plotted in Fig. 3.6 shows a loss in energy at order-limit $M = 5$. Furthermore, reconstructing the spectral coefficients using $M = 5$ results in a reconstruction error of the order $10^{-16}$. Representing the signal in (3.11) using the proposed scheme requires $(L)(2M + 1) = 308$ samples whereas the 'non-order-limited' GL method requires $(L)(2L - 1) = 1540$ samples. This comparison is visualized in Fig. 3.7.

## 3.3 Conclusion

For signals on the sphere that exhibit approximate rotational symmetry, we have presented an order-limited Gauss-Legendrian sampling method and developed the associated SHTs. We have also analyzed the precisional and computational aspects of the proposed sampling scheme and shown that the proposed sampling enables accurate and efficient computation of SHT as evidenced by negligible reconstruction errors. We have also demonstrated the utility of the proposed method for sampling and reconstruction of antenna radiation signals.

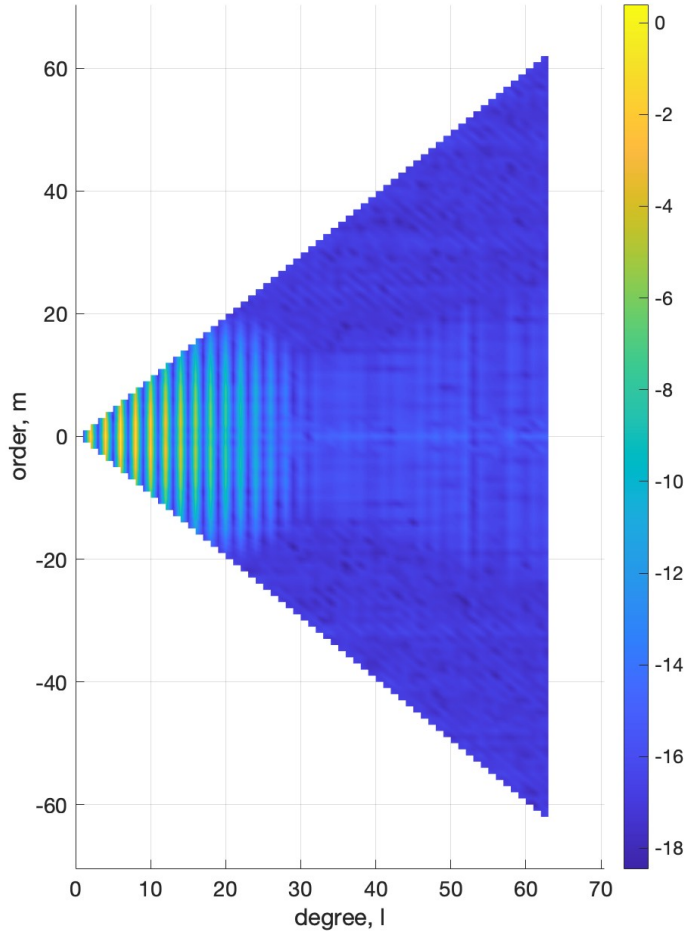


Figure 3.5: Antenna radiation pattern in the spherical harmonic domain (GL)

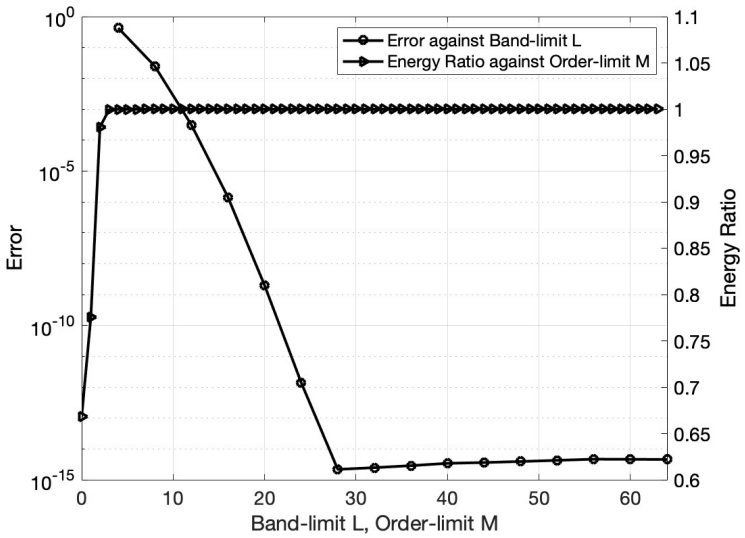


Figure 3.6: Reconstruction error and energy ratio of the perturbed radiation pattern (GL)

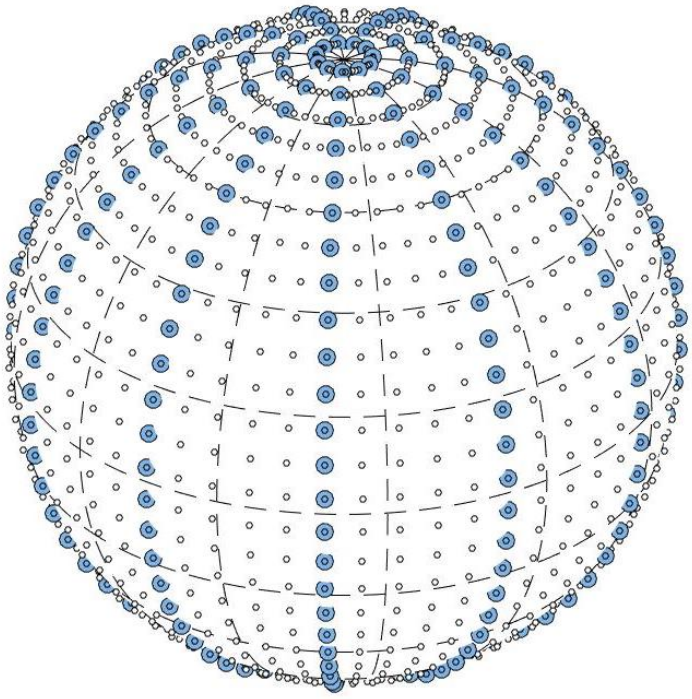

Figure 3.7: Sampling map with (blue) and without (white) order-limiting for $L = 28$, $M = 5$ (GL)

# Chapter 4

# Order-limiting Optimal Dimensionality Samples

Spherical signal processing includes signal processing in spatial and spectral domains that are linked to each other via the well-known Spherical Harmonic Transform (SHT) [22, 27, 36]. Since datasets may be very large [2], sample acquisition on the sphere must have the least sampling number requirement for accurate and efficient computation of SHT. This study investigates the advantages of computing a subset of spherical coefficients instead of all coefficients for applications that make use of signals that are nearly azimuthally symmetric (NAS). This is particularly useful for antenna radiation patterns [35], as any degradation in the axial symmetry can lead to modeling errors. We propose a framework for accurate representation of such signals by order-limiting the band-limited signals. Although there is literature on spherical sampling schemes and efficient computation of the SHT [20, 22–27, 29, 31, 32], we demonstrate the utility of order-limiting for NAS signals using the Optimal Dimensionality (OD) sampling scheme.

## 4.1 The Sampling Scheme

We consider a problem to design a method – using the OD sampling scheme – for the sampling of order-limited signals such that SHT of the signal can be computed accurately and efficiently. None of the existing sampling techniques exploit the order-limiting potential of an NAS signal to reduce the number of samples while maintaining SHT accuracy.

### 4.1.1 Harmonic Formulation

A signal $L^2(\mathbb{S}^2)$ exhibits azimuthal symmetry if $f(\theta,\phi) = f(\theta)$. Azimuthally symmetric signals (a special form of rotationally symmetric signals with z-axis as axis of rotation) form a subspace denoted by $\mathcal{H}_0 \subseteq L^2(\mathbb{S}^2)$. For $f \in \mathcal{H}_0$, $(f)_l^m = 0$ for $m \neq 0$, which implies that an azimuthally symmetric signal is expanded using zero-order spherical harmonics.
A spherical signal $f(\theta,\phi) \in L^2(\mathbb{S}^2)$ is band-limited to degree $L$ if $(f)_\ell^m = 0, \forall\, \ell \geq L$. Such signals form an $L^2$ dimensional subspace denoted by $\mathcal{H}_L \subseteq L^2(\mathbb{S}^2)$. Furthermore, a spherical signal $f(\theta,\phi) \in \mathcal{H}_L$ is considered to be order-limited at $M < L$ if $(f)_\ell^m = 0 \;\forall\; \ell \geq L, m > M$, and therefore can be represented as

$$f(\theta,\phi) = \sum_{\ell=0}^{L-1} \sum_{m=-N}^{N} (f)_\ell^m Y_\ell^m(\theta,\phi), \quad N = \min(\ell, M). \tag{4.1}$$

The signals of the form given in (4.1) make $M^2+(L-M)(2M+1)$ subspace denoted by $\mathcal{H}_{LM} \subseteq \mathcal{H}_L$. It follows that $\mathcal{H}_{LM} \subset \mathcal{H}_L \;\forall\; M < L$. By expressing the spherical harmonic basis of degree $\ell$ and order $m$ as

$$Y_\ell^m(\theta,\phi) = \widetilde{Y}_\ell^m(\theta) e^{-im\phi}, \tag{4.2}$$

and defining $F_m(\theta)$ as

$$F_m(\theta) = \int_{\phi=0}^{2\pi} f(\theta,\phi) e^{-im\phi}, \tag{4.3}$$

we reformulate SHT given in (2.16) as

$$(f)_\ell^m = \int_{\theta=0}^{\pi} F_m(\theta) \widetilde{Y}_\ell^m(\theta) \sin\theta d\theta, \tag{4.4}$$

We can use (4.3) and (4.4) to compute SHT, provided the integrals can be discretized and evaluated accurately.

### 4.1.2 Proposed Sampling Scheme and Spherical Harmonic Transform

A vector of thetas corresponding to the equi-spaced co-latitude gradations on the sphere are defined as

$$\boldsymbol{\theta} \triangleq [\theta_0, \theta_1, \ldots, \theta_{L-1}]^T. \tag{4.5}$$

Let $k$ be the variable that indexes the rings corresponding to the points in (4.5). A

ring located at point $k$ has a vector $\phi^k$ of equi-spaced longitudinal points defined as

$$\phi^k \triangleq [0, \Delta_k, 2\Delta_k, \ldots, (2N)\Delta_k], \quad \Delta_k = \frac{2\pi}{2N+1}, \tag{4.6}$$

where $N = \min(k, M)$. Much like its Gauss-Legendre counterpart, this sampling scheme has $L$ latitude points. The number of longitudinal points in each ring depends on the location of the ring along latitude for the first $M$ rings, and becomes constant (order-limited) afterwards. The spatial dimensionality of this scheme is

$$\left[\sum_{k=0}^{M}(2k+1)\right] + (L-M-1)(2M+1) = N_{\mathrm{OOL}}, \tag{4.7}$$

which simplifies to $M^2 + (L-M)(2M+1)$ and is referred to as $N_{\mathrm{OOL}}$, where OOL stands for optimal-order-limited. Like its 'non-order-limited' version, the spatial dimensionality of the order-limited OD sampling scheme is equal to its harmonic degrees of freedom.

We show the mathematical formulation of the analysis and synthesis equations for a spherical signal $f(\theta, \phi)$ sampled with $N_{OOL}$ spatial dimensionality before presenting their algorithms.

A vector $\mathbf{g}_m$ for orders $|m| < L$ is defined as

$$\mathbf{g}_m \equiv G_m\left(\boldsymbol{\theta}^m\right) \triangleq \left[G_m\left(\theta_{|m|}\right), G_m\left(\theta_{|m|+1}\right), G_m\left(\theta_{L-1}\right)\right]^T, \tag{4.8}$$

where $G_m(\theta_k)$ is defined for each equi-spaced latitude ring $\theta_k \in \boldsymbol{\theta}$ as

$$\begin{aligned} G_m(\theta_k) &\triangleq \int_0^{2\pi} f(\theta_k, \phi)\, e^{-im\phi} d\phi \\ &= 2\pi \sum_{\ell=m}^{L-1} (f)_\ell^m \tilde{P}_\ell^m(\theta_k), \end{aligned} \tag{4.9}$$

with $\tilde{P}_\ell^m(\theta) \triangleq Y_\ell^m(\theta, 0)$ as the scaled associated canonical Legendre functions. We define a matrix $\mathbf{P}_m$ as

$\mathbf{P}_m \triangleq 2\pi$

$$\begin{pmatrix} \tilde{P}^m_{|m|}\left(\theta_{|m|}\right) & \tilde{P}^m_{|m|+1}\left(\theta_{|m|}\right) & \cdots & \tilde{P}^m_{L-1}\left(\theta_{|m|}\right) \\ \tilde{P}^m_{|m|}\left(\theta_{|m|+1}\right) & \tilde{P}^m_{|m|+1}\left(\theta_{|m|+1}\right) & \cdots & \tilde{P}^m_{L-1}\left(\theta_{|m|+1}\right) \\ \vdots & \vdots & \ddots & \vdots \\ \tilde{P}^m_{|m|}\left(\theta_{L-1}\right) & \tilde{P}^m_{|m|+1}\left(\theta_{L-1}\right) & \cdots & \tilde{P}^m_{L-1}\left(\theta_{L-1}\right) \end{pmatrix}, \tag{4.10}$$

and a vector of harmonic factors of orders $m \leq |M|$ as

$$\mathbf{f}_m = \left[(f)^m_{|m|}, (f)^m_{|m|+1}, \ldots, (f)^m_{L-1}\right]^T. \tag{4.11}$$

The matrices in equations (4.8), (4.10) and (4.11) are related by the following expression:

$$\mathbf{g}_m = \mathbf{P}_m \mathbf{f}_m. \tag{4.12}$$

The spectral triangle in Fig. 4.1 shows a plot of the spherical harmonic coefficients against the band-limit. The coefficients $(f)^{L-1}_{L-1}$ and $(f)^{-(L-1)}_{-(L-1)}$ of orders $L-1$ and $-(L-1)$ respectively can be determined from (4.12). Once we have these coefficients, the signal can be updated as

$$f(\theta, \phi) \leftarrow f(\theta, \phi) - \tilde{f}_{L-1}(\theta, \phi), \tag{4.13}$$

where

$$\begin{aligned} \tilde{f}_m(\theta, \phi) &= \sum_{\ell=m}^{L-1} \left((f)^m_\ell Y^m_\ell(\theta, \phi) + (f)^{-m}_\ell Y^{-m}_\ell(\theta, \phi)\right) \\ &= \sum_{\ell=m}^{L-1} \left((f)^m_\ell \tilde{P}^m_\ell(\theta) e^{im\phi} + (f)^{-m}_\ell \tilde{P}^{-m}_\ell(\theta) e^{-im\phi}\right) \\ &= \frac{1}{2\pi}\left(e^{im\phi} G_m(\theta) + e^{-im\phi} G_{-m}(\theta)\right) \end{aligned} \tag{4.14}$$

is the spatial share of the coefficients of orders $m$ and $-m$ and all degrees $m \leq \ell \leq (L-1)$. The updating iteration is repeated until $L$ becomes equal to zero. The inverse is computed as

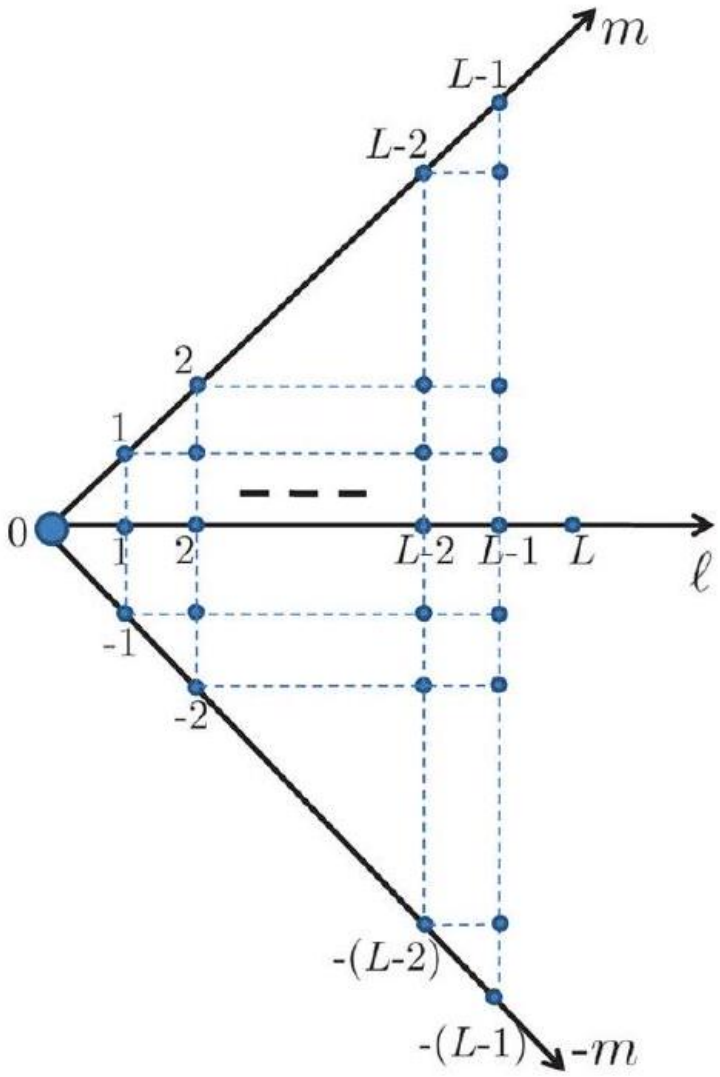


Figure 4.1: Spectral graph of a band-limited signal

$$\begin{aligned} f(\theta,\phi) &= \frac{1}{2\pi}\sum_{m=-M}^{M} e^{im\phi} G_m(\theta) \\ &= \sum_{m=0}^{M} \tilde{f}_m(\theta,\phi), \end{aligned} \tag{4.15}$$

where $M$ is the order-limit of the signal. Using the method mentioned above, the proposed SHTs are summarized in the form of Algorithms 3 and 4.

### 4.1.3 Numerical Accuracy Analysis

To analyse the accuracy of the transforms, we generate a band-limited and order-limited signal $f_{\mathrm{BOL}} \in \mathcal{H}_{LM}$ by randomly initializing complex numbers of unity

**Algorithm 3** Forward SHT

**Require:** $(f)_\ell^m \ \forall\ 0 \leq \ell \leq (L-1), |m| \leq \min(\ell, M)$

**procedure** FORWARD-SHT($f(\theta, \phi)$)
  initialize $(f)_\ell^m$ vector of size $M^2 + (L-M)(2M+1)$
  **for** $\ell = L-1, L-2, .., 0$ **do**
    compute $\mathbf{g}_m$ and $\mathbf{g}_{-m}$ by evaluating $G_m(\theta)$ and $G_{-m}(\theta)$ for all $\theta_k \in \boldsymbol{\theta}^m$ by taking $(2m+1)$ point FFT along each $\phi$-ring
    evaluate $\mathbf{P}_m$ and $\mathbf{P}_{-m}$, using $\mathbf{P}_{-m} = (-1)^m \mathbf{P}_m$
    compute $\mathbf{f}_m$ and $\mathbf{f}_{-m}$ by inverting (4.12)
    determine $\tilde{f}_m(\theta, \phi)$ for all $\theta_k \in \boldsymbol{\theta} \backslash \boldsymbol{\theta}^m$ and all associated sampling points along $\phi$
    update $f(\theta, \phi) \leftarrow f(\theta, \phi) - \tilde{f}_m(\theta, \phi)$ for all $\theta_k \in \boldsymbol{\theta} \backslash \boldsymbol{\theta}^m$ and all associated sampling points along $\phi$
  **end for**
  **return** $(f)_\ell^m$
**end procedure**

**Algorithm 4** Inverse SHT

**Require:** $f(\theta, \phi)$

**procedure** INVERSE-SHT($(f)_\ell^m$)
  initialize $f(\theta, \phi) = 0$
  **for** $m = 0, 1, \ldots, M$ **do**
    evaluate $\tilde{P}_\ell^m(\theta_k)$ and $\tilde{P}_\ell^{-m}(\theta_k)$ for all $\theta_k \in \boldsymbol{\theta}$ and $m \leq \ell \leq (L-1)$
    compute $G_m(\theta_k)$ and $G_{-m}(\theta_k)$ for all $\theta_k \in \boldsymbol{\theta}$
    compute $\tilde{f}_m(\theta, \phi)$ for all sampling points
    update $f(\theta, \phi) \leftarrow f(\theta, \phi) + \tilde{f}_m(\theta, \phi)$ for all sampling points
  **end for**
  **return** $f(\theta, \phi)$
**end procedure**

magnitude as its harmonic factors $(f_{\mathrm{BOL}})_\ell^m$ for $0 < \ell < L, |m| \leq \min(\ell, M)$. We synthesize the spatial signal by inverse SHT for $4 \leq L \leq 512$ and $M = L/2$. This is followed by a forward transform to obtain reconstructed harmonic factors referred to as $(f_r)_\ell^m$. This is repeated ten times to record the average value for the mean and maximum errors $E_{\mathrm{mean}}$ and $E_{\mathrm{max}}$ given by

$$E_{\mathrm{mean}} = \frac{1}{L^2} \sum_{\ell=0}^{L-1} \sum_{m=-\min(\ell,M)}^{\min(\ell,M)} |(f_{\mathrm{BOL}})_\ell^m - (f_r)_\ell^m| \,, \tag{4.16}$$

$$E_{\mathrm{max}} = \max |(f_{\mathrm{BOL}})_\ell^m - (f_r)_\ell^m| \,, \tag{4.17}$$

which are plotted in Fig. 4.2. We also plot the reconstruction error $|(f_{\mathrm{BOL}})_\ell^m - (f_r)_\ell^m|$ for one realization, $L = 512$ and $M = 256$ on a base-10 logarithmic scale in Fig. 4.3. These plots indicate that the proposed order-limited OD sampling method and its SHTs allow signal reconstruction with negligible errors.

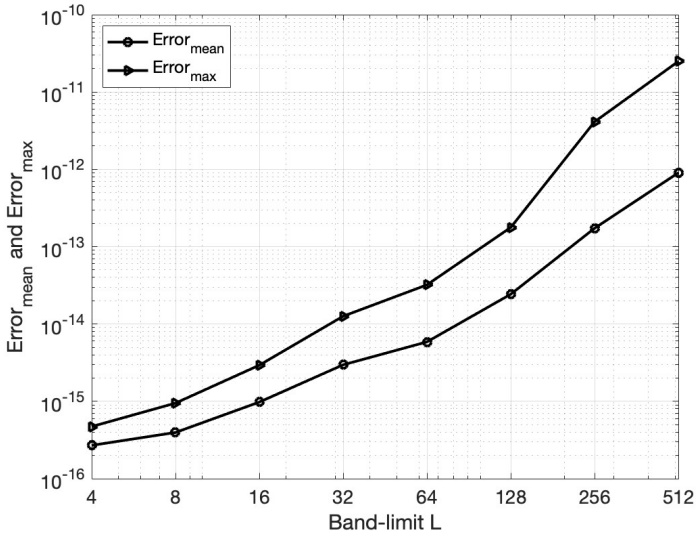


Figure 4.2: Mean and maximum reconstruction errors (OD)

### 4.1.4 Computational Complexity

The time required to compute the proposed transforms for order-limited signals are shown in Fig. 4.4. These are plotted for band-limits $4 \leq L \leq 512$ while limiting the order at $L/2 \; \forall \; L$. The times are averaged over 10 random signals and measured in MATLAB running on a laptop computer equipped with 2.7 GHz Intel Core i5 processor with 8 GB RAM. The experimental times for the transforms evolve with the band-limit as $O\left(L\left(M^2 + (L-M)(2M+1)\right)\right)$ – which is the theoretical

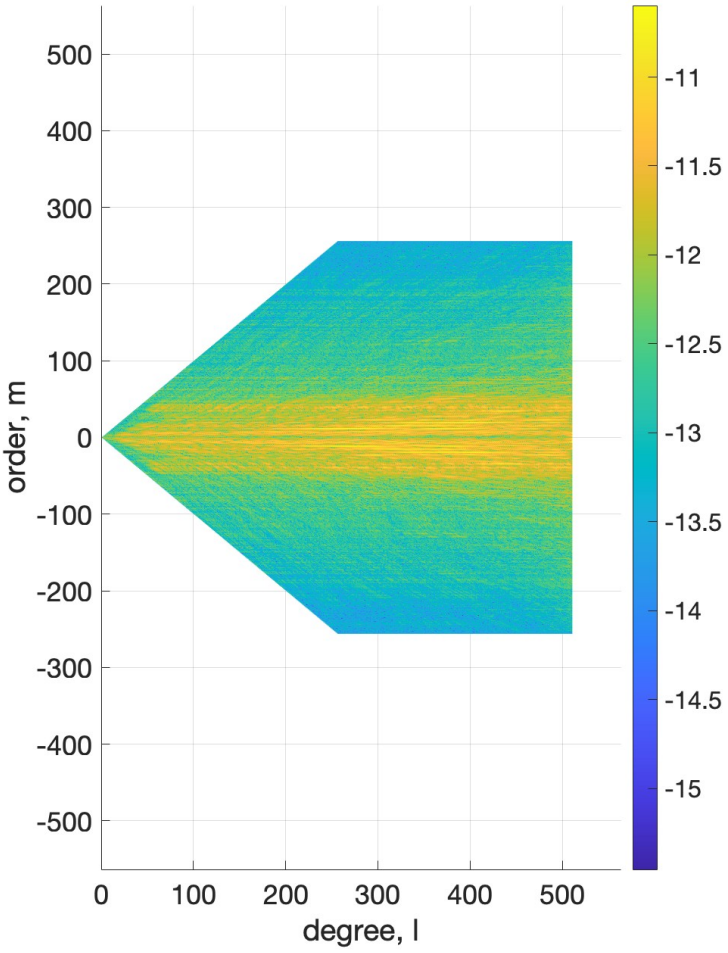


Figure 4.3: Reconstruction error for $L = 512$, $M = 256$ (OD)

computational complexity of the proposed transforms – increases linearly with the band-limit. We note that the complexity of the proposed transforms is less than the complexity $O\left(L^3\right)$ of the SHTs associated with the sampling methods that do not exploit the order-limiting potential of a signal.

## 4.2 Application: Sampling Antenna Radiation Pattern

We consider a dipole antenna radiation pattern with perfect azimuthal symmetry defined in [38] as

$$r(\theta, \phi) = \left| \frac{\cos(kY\cos(\theta)/2) - \cos(kY/2)}{\sin(\theta)} \right|^2, \tag{4.18}$$

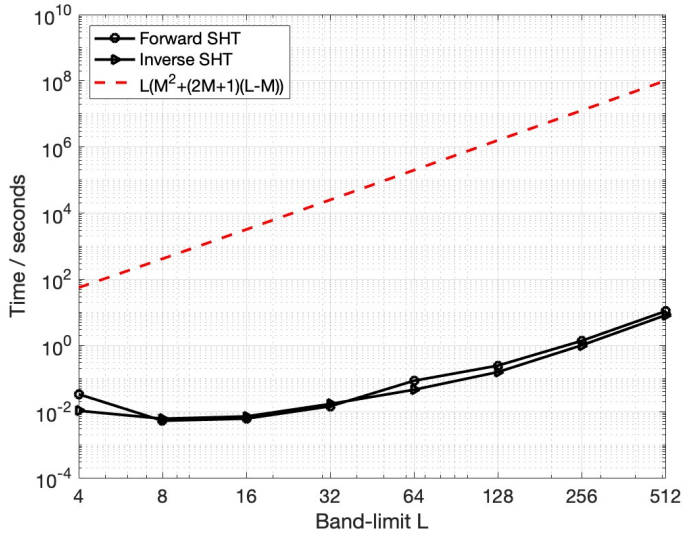


Figure 4.4: Time complexity analysis of forward and inverse transforms (OD)

where $k$ is the phase constant and $Y$ is the antenna length. Here, $k$ and $Y$ are taken as $\frac{2\pi}{\lambda}$ and $1.4\lambda$ respectively, where $\lambda$ is the wavelength taken to be 1.0 m. We introduce random rotational perturbations to model the fact that the radiation pattern is not perfectly AS in practice, that is,

$$\tilde{r}(\theta,\phi) = \frac{1}{P}\sum_{i=1}^{P} D\left(\alpha_i,\beta_i\right) r(\theta,\phi), \tag{4.19}$$

where $D(\alpha,\beta)$ is a Wigner-D like operator that rotates the signal by $\beta$ around $y$-axis followed by an $\alpha$ rotation around $z$-axis. We choose both $\alpha_i, \beta_i$ uniformly distributed in $[0,\pi/6]$ for $P = 10$ rotations to corrupt the perfectly AS signal, thus rendering it NAS. The radiation pattern $\tilde{r}(\theta,\phi)$ is plotted in spatial and spectral domains in Fig. 4.5 and Fig. 4.6 respectively.

In order to find the band-limit of the perturbed signal, we analyze the reconstruction error, plotted in Fig. 4.7, for different band-limits and choose $L = 28$ as an effective band-limit of the signal. In order to find order-limit of the signal, we take the ratio of energies of spectral coefficients of the order and band-limited signal with respect to the band-limited signal only, so as to gauge the significant loss of energy when reducing the order-limit of the signal. Upon reducing the order of the signal, this energy ratio plotted in Fig. 4.7 shows a loss in energy at order-limit $M = 5$. Furthermore, reconstructing the spectral coefficients using $M = 5$ results in a reconstruction error of the order $10^{-15}$. Representing the signal in (4.19) using the proposed scheme requires $M^2 + (L-M)(2M+1) = 322$ samples whereas the 'non-order-limited' OD method requires $L^2 = 1024$ samples. This comparison is

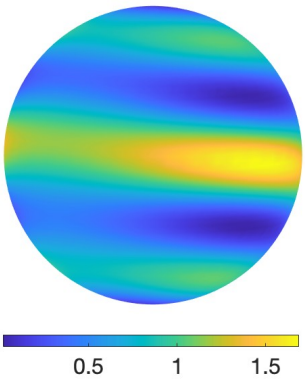


Figure 4.5: Antenna radiation pattern in the spatial domain (OD)

visualized in Fig. 4.8.

## 4.3 Conclusion

For signals on the sphere that exhibit approximate rotational symmetry, we have presented an order-limited OD sampling method and developed the associated SHTs. We have also analyzed the precisional and computational aspects of the proposed sampling scheme and shown that the proposed sampling enables accurate and efficient computation of SHT as evidenced by negligible reconstruction errors. We have also demonstrated the utility of the proposed method for sampling and reconstruction of antenna radiation signals.

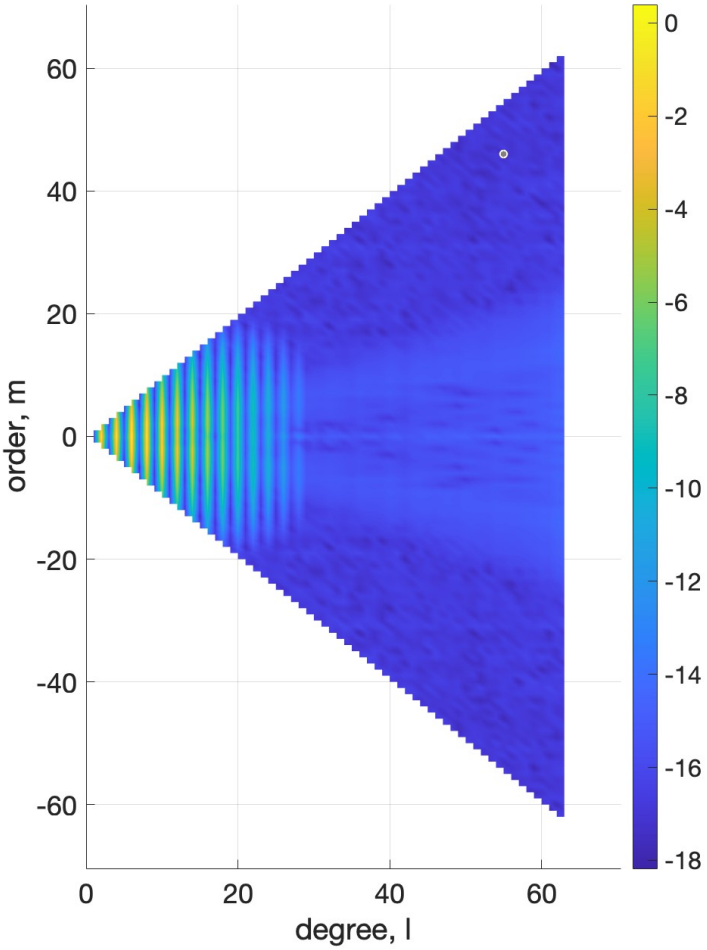


Figure 4.6: Antenna radiation pattern in the spectral domain (OD)

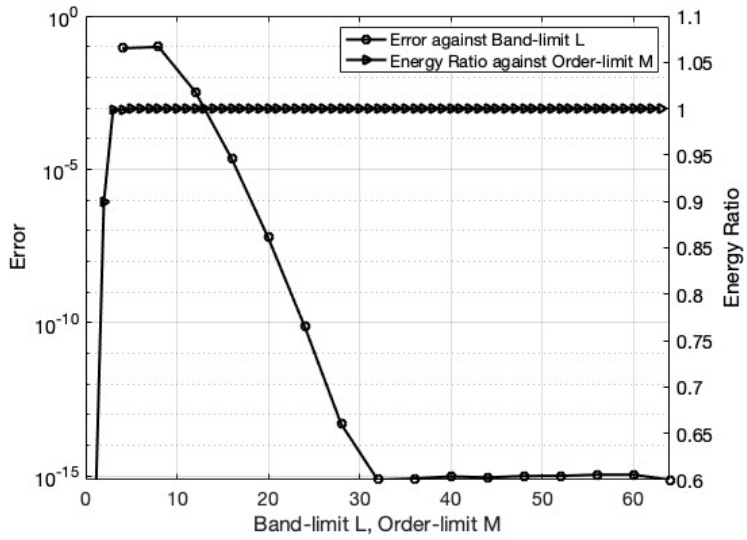


Figure 4.7: Reconstruction error and energy ratio of the perturbed radiation pattern (OD)

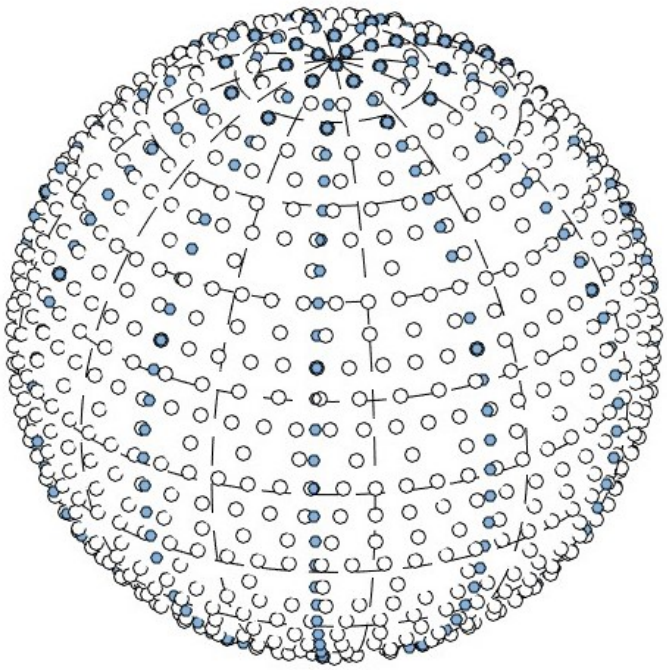

Figure 4.8: Sampling map with (blue) and without (white) order-limiting for $L = 32$, $M = 5$ (OD)

# Chapter 5

# Summary and Future Research Directions

This research work explores the problem of order-limited sampling in the spherical domain for accurate computation of spherical harmonic transform (SHT). Nearly azimuthally symmetric (NAS) signals form a class of signals which do not have significant information content in higher spectral orders. We showed that by limiting the spectral order, we can accurately represent this class of signals using fewer samples. A framework for accurate representation of NAS signals was presented, alongwith an application which incorporated this proposed framework, thus proving its validity. Algorithms for the SHTs for the proposed framework were also presented. Their accuracy was demonstrated by multiple trials of random signal reconstruction error plots.

The order-limiting functionality of SHTs can be applied to other sampling schemes to make use of its reduced computational expenditure. It can be tested on other applications which involve spherical functions with near azimuthal symmetry. The order-limiting concept can also be extended to NAS signals rotated by Wigner-D functions and spatially limited by Slepian functions.

# References


[1] Frederik Simons and F. Dahlen, "Spherical slepian functions and the polar gap in geodesy," *Geophysical Journal International*, vol. 166, 03 2006.

[2] Wen Zhang, Mengqiu Zhang, Rodney Kennedy, and Thushara Abhayapala, "On high-resolution head-related transfer function measurements: An efficient sampling scheme," *IEEE Transactions on Audio Speech and Language Processing*, vol. 20, pp. 575–584, 02 2012.

[3] Alastair Moore, Christine Evers, and Patrick Naylor, "Direction of arrival estimation in the spherical harmonic domain using subspace pseudo-intensity vectors," *IEEE/ACM Transactions on Audio, Speech, and Language Processing*, vol. PP, pp. 1–1, 09 2016.

[4] Ren Ng, Ravi Ramamoorthi, and Pat Hanrahan, "Triple product wavelet integrals for all-frequency relighting," *ACM Transactions on Graphics*, vol. 23, 07 2004.

[5] Ping-Man Lam, Chi-Sing Leung, and Tien-Tsin Wong, "Noise-resistant fitting for spherical harmonics," *IEEE transactions on visualization and computer graphics*, vol. 12, pp. 254–65, 03 2006.

[6] F. Dahlen and Frederik Simons, "Spectral estimation on a sphere in geophysics and cosmology," *Geophysical Journal International*, vol. 174, 05 2007.

[7] T.E.J. Behrens and Saad Jbabdi, "Diffusion mri: from quantitative measurement to in vivo neuroanatomy," *MR Diffusion Tractography*, pp. 333–351, 11 2013.

[8] J. Weiland, N. Odegard, R. Hill, Edward Wollack, G. Hinshaw, M. Greason, N. Jarosik, Lyman Page, C. Bennett, J. Dunkley, Ben Gold, M. Halpern, A. Kogut, Eiichiro Komatsu, D. Larson, Maestreq Limón, Stephan Meyer, M. Nolta, K. Smith, and and Wright, "Seven-year wilkinson microwave anisotropy probe (wmap) observations: Planets and celestial calibration

sources," *The Astrophysical Journal Supplement Series*, vol. 192, pp. 19, 01 2011.

[9] Planck Collaboration, Yashar Akrami, F. Arroja, M. Ashdown, Jonathan Aumont, Carlo Baccigalupi, Mario Ballardini, A. Banday, Ramon Barreiro, N. Bartolo, Souvik Basak, Richard Battye, K. Benabed, J. Bernard, M. Bersanelli, P. Bielewicz, J. Bock, J. Bond, J. Borrill, and A. Zonca, "Planck 2018 results. i. overview and the cosmological legacy of planck," 07 2018.

[10] Marcus Johansson and Valera Veryazov, "Automatic procedure for generating symmetry adapted wavefunctions," *Journal of Cheminformatics*, vol. 9, 02 2017.

[11] Tony Pollock, Thushara Abhayapala, and Rodney Kennedy, "Introducing space into mimo capacity calculations," *Telecommunication Systems*, vol. 24, pp. 415–436, 10 2003.

[12] Qurrat-Ul-Ain Nadeem, Abla Kammoun, mérouane Debbah, and Mohamed-Slim Alouini, "A generalized spatial correlation model for 3d mimo channels based on the fourier coefficients of power spectrums," *IEEE Transactions on Signal Processing, to appear*, vol. 63, 04 2015.

[13] Jet Propulsion Laboratory / National Aeronautics and Space Administration, "Global climate change: Evidence," 2008.

[14] Ting-Hang Pei, "Different explanations for the cosmic microwave background radiation," 10 2021.

[15] F. Argüeso, J. González-Nuevo, J. L. Sanz, L. Toffolatti, P. Vielva, D. Herranz, and M. López-Caniego, "The mexican hat wavelet family. application to point source detection in cosmic microwave background maps," in *2005 13th European Signal Processing Conference*, 2005, pp. 1–4.

[16] A. Doroshkevich, P Naselsky, O. Verkhodanov, D Novikov, V Turchaninov, I Novikov, P Christensen, and Lung-Yih Chiang, "Gauss–legendre sky pixelization (glesp) for cmb maps," *Int. J. of Modern Physics D*, vol. 14, pp. 275, 01 2005.

[17] Moo K. Chung, Kim M. Dalton, and Richard J. Davidson, "Tensor-based cortical surface morphometry via weighted spherical harmonic representation," *IEEE Transactions on Medical Imaging*, vol. 27, no. 8, pp. 1143–1151, 2008.

[18] Huaping Liu, Yong Fang, and Qinghua Huang, "Efficient representation of head-related transfer functions with combination of spherical harmonics and spherical wavelets," *IEEE Access*, vol. 7, pp. 78214–78222, 2019.

[19] United States Government, "Wright-patterson air force base official website," 1917.

[20] Zubair Khalid, Rodney A. Kennedy, and Jason D. McEwen, "An optimal-dimensionality sampling scheme on the sphere with fast spherical harmonic transforms," *IEEE Transactions on Signal Processing*, vol. 62, no. 17, pp. 4597–4610, 2014.

[21] Alice P. Bates, Zubair Khalid, and Rodney A. Kennedy, "Slepian spatial-spectral concentration problem on the sphere: Analytical formulation for limited colatitude–longitude spatial region," *IEEE Transactions on Signal Processing*, vol. 65, no. 6, pp. 1527–1537, 2017.

[22] James Driscoll and Dennis Healy, "Computing fourier transforms and convolutions on the 2-sphere," *Advances in Applied Mathematics*, vol. 15, 06 1994.

[23] Nico Sneeuw, "Global spherical harmonic analysis by least-squares and numerical quadrature methods in historical perspective," *Geophysical Journal International*, vol. 118, pp. 707 – 716, 09 1994.

[24] Robert Crittenden and Neil Turok, "Exactly azimuthal pixelizations of the sky," 07 1998.

[25] Martin Mohlenkamp, "A fast transform for spherical harmonics," *The Journal of Fourier Analysis and Applications*, vol. 5, 07 1999.

[26] D. Jr, D. Rockmore, P.J. Kostelec, and S.S.B. Moore, "Ffts for the 2-sphere-improvements and variations," *The Journal of Fourier Analysis and Applications*, vol. 9, pp. 341–385, 01 1998.

[27] Jason McEwen and Yves Wiaux, "A novel sampling theorem on the sphere," *Signal Processing, IEEE Transactions on*, vol. 59, pp. 5876 – 5887, 01 2012.

[28] Jens Keiner, Stefan Kunis, and Daniel Potts, "Efficient reconstruction of functions on the sphere from scattered data," *PAMM*, vol. 13, pp. 435–458, 01 2007.

[29] Peter Kostelec and Daniel Rockmore, "Ffts on the rotation group," *Journal of Fourier Analysis and Applications*, vol. 14, pp. 145–179, 04 2008.

[30] Jason McEwen, "Fast, exact (but unstable) spin spherical harmonic transforms," 07 2008.

[31] Krzysztof Gorski, Eric Hivon, AJ Banday, Benjamin Wandelt, F. Hansen, M. Reinecke, and M. Bartelman, "Healpix: A framework for high-resolution discretization and fast analysis of data distributed on the sphere," *apj*, vol. 622, 09 2004.

[32] Rod Blais and Muhammad Soofi, "Spherical harmonic transforms using quadratures and least squares," 05 2006, pp. 48–55.

[33] W Skukowsky, "A quadrature formula over the sphere with application to high resolution spherical harmonic analysis," *J. Geodesy*, vol. 60, pp. 1–14, 03 1986.

[34] Alice Bates, Zubair Khalid, and Rodney Kennedy, "Novel sampling scheme on the sphere for head-related transfer function measurements," *IEEE/ACM Transactions on Audio, Speech, and Language Processing*, vol. 23, pp. 1068–1081, 06 2015.

[35] Fernando Rodríguez Varela, Xiaoliang Sun, Belén Galocha Iragüen, and Manuel Sierra Castañer, "Reduced azimuthal sampling for spherical near-field measurements," in *2020 Antenna Measurement Techniques Association Symposium (AMTA)*, 2020, pp. 1–5.

[36] R. A. Kennedy and P. Sadeghi, *Hilbert Space Methods in Signal Processing*, Cambridge University Press, Cambridge, UK, March 2013.

[37] Dag Seljebotn and Hans Eriksen, "Sympix: A spherical grid for efficient sampling of rotationally invariant operators," *The Astrophysical Journal Supplement Series*, vol. 222, 04 2015.

[38] Constantine A Balanis, *Antenna theory: analysis and design*, Wiley-Interscience, 2005.